PALEOCEANOGRAPHY

Active Pacific meridional overturning circulation (PMOC) during the warm Pliocene

Natalie J. Burls,[1,2]* Alexey V. Fedorov,[2] Daniel M. Sigman,[3] Samuel L. Jaccard,[4] Ralf Tiedemann,[5] Gerald H. Haug[6,7]

An essential element of modern ocean circulation and climate is the Atlantic meridional overturning circulation (AMOC), which includes deep-water formation in the subarctic North Atlantic. However, a comparable overturning circulation is absent in the Pacific, the world's largest ocean, where relatively fresh surface waters inhibit North Pacific deep convection. We present complementary measurement and modeling evidence that the warm, ~400–ppmv (parts per million by volume) CO_2 world of the Pliocene supported subarctic North Pacific deep-water formation and a Pacific meridional overturning circulation (PMOC) cell. In Pliocene subarctic North Pacific sediments, we report orbitally paced maxima in calcium carbonate accumulation rate, with accompanying pigment and total organic carbon measurements supporting deep-ocean ventilation-driven preservation as their cause. Together with high accumulation rates of biogenic opal, these findings require vigorous bidirectional communication between surface waters and interior waters down to ~3 km in the western subarctic North Pacific, implying deep convection. Redox-sensitive trace metal data provide further evidence of higher Pliocene deep-ocean ventilation before the 2.73-Ma (million years) transition. This observational analysis is supported by climate modeling results, demonstrating that atmospheric moisture transport changes, in response to the reduced meridional sea surface temperature gradients of the Pliocene, were capable of eroding the halocline, leading to deep-water formation in the western subarctic Pacific and a strong PMOC. This second Northern Hemisphere overturning cell has important implications for heat transport, the ocean/atmosphere cycle of carbon, and potentially the equilibrium response of the Pacific to global warming.

INTRODUCTION

The Pliocene [2.58 to 5.33 million years ago (Ma)] is the most recent epoch in geological history during which atmospheric CO_2 concentrations were comparable to those of today [350 to 400 parts per million (ppm) by volume] (*1*, *2*), and therefore may offer insight into future climate change as Earth continues to warm. One key process in global and regional climate is the ocean meridional overturning circulation, which affects poleward heat transport, nutrient cycles, and the air-sea exchange of carbon dioxide. This circulation depends, to a large degree, on deep-water formation, which, in today's climate, occurs in the high latitudes of the North Atlantic basin but not the North Pacific.

The absence of deep-water formation in the modern North Pacific has been attributed primarily to the relatively fresh surface conditions in the subarctic North Pacific (SNP) (*3*). These conditions are, in turn, best explained by the local excess of precipitation over evaporation in the northern Pacific due to net moisture transport from the Atlantic to the Pacific (*4*) and/or moisture transport associated with the Asian monsoon (*5*). Some studies link the lack of deep-water formation in the Pacific directly to its occurrence in the Atlantic via the Atlantic-Pacific seesaw effect (*6*), while idealized experiments indicate that the smaller width of the Atlantic predisposes it to higher salinity and deep-water formation (*7*). Here, we present new observational and experimental results demonstrating that deep water formed in the North Pacific during the warm Pliocene, with both North Atlantic Deep Water (NADW) and North Pacific Deep Water (NPDW) formation active at that time.

[1]Center for Ocean-Land-Atmosphere Studies, Department of Atmospheric, Oceanic, and Earth Sciences, George Mason University, Fairfax, VA 22030, USA. [2]Department of Geology and Geophysics, Yale University, New Haven, CT 06511, USA. [3]Department of Geosciences, Princeton University, Princeton, NJ 08544, USA. [4]Institute of Geological Sciences and Oeschger Center for Climate Change Research, University of Bern, Bern, Switzerland. [5]Alfred Wegener Institute, Bremerhaven, Germany. [6]Department of Climate Geochemistry, Max-Planck Institute for Chemistry, Mainz, Germany. [7]Geological Institute, Department of Earth Sciences, ETH Zürich, Switzerland.
*Corresponding author. Email: nburls@gmu.edu

RESULTS

In the western SNP [Ocean Drilling Program (ODP) Site 882], the accumulation rates of biogenic opal and alkenones were remarkably high throughout most of the Pliocene, declining sharply upon the intensification of Northern Hemisphere glaciation at 2.73 Ma [Fig. 1, A to C; (*8*, *9*)]. Together with reduced Pliocene nitrate consumption, these observations indicate a substantially higher rate of the gross input of nutrient-rich subsurface water into the SNP surface (*9*, *10*). Biogenic opal production in the polar ocean requires vertical circulation that carries silicate-rich deep water into the euphotic zone. Dissolved silicate supply to the SNP surface can be achieved by the input of subsurface waters from a range of depths, although very deep mixing would be required to tap the depth maximum in silicate concentration, which occurs at ~1700 m in the modern North Pacific. Accordingly, the high Pliocene accumulation of opal indicates that silicate was being imported rapidly into the surface waters of the western SNP, for which there are three possible explanations: (i) rapid Ekman upwelling, (ii) wintertime mixing that reached only a few hundred meters, or (iii) deep wintertime convection that reached into the deep ocean (thousands of meters), possibly to the seafloor.

Observations of calcium carbonate ($CaCO_3$) content and accumulation rate extending back to 6 Ma at ODP Site 882 allow us to distinguish among these possibilities (Fig. 1, D and E). Previous work from this site covering the last 800 ky (thousand years) of the Pleistocene identified spikes in $CaCO_3$ (to ~25% by weight) at the deglacials and early interglacials (*11*). These spikes have been explained as the result of greater deep-ocean ventilation, with both the North Pacific and Southern Ocean as potential contributors to this ventilation (*12*, *13*). The data

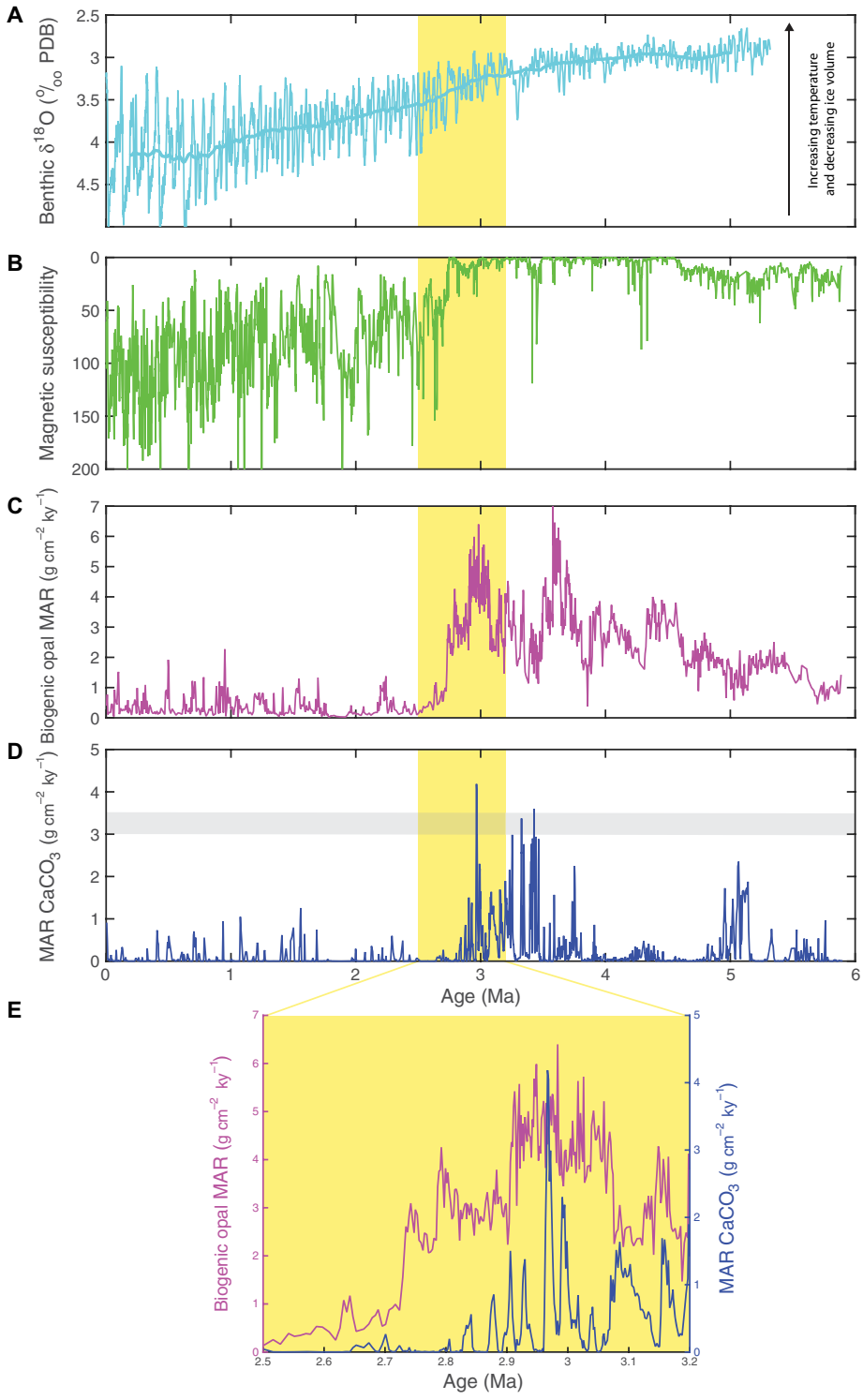

Fig. 1. Changes in Northern Pacific climate over the last 6 million years. (**A**) Benthic $\delta^{18}O$ record (*62*) showing glacial cycles in global ice volume and deep-ocean temperature with smoothed trend line superimposed. PDB, Pee Dee Belemnite. (**B**) Magnetic susceptibility of ocean sediments at ODP Site 882 (*8*) in the subarctic Pacific (see Fig. 3 for site location). This nondimensional variable increases in the presence of ice-rafted debris from Northern Hemisphere glaciers. (**C**) Biogenic opal (*8*) and (**D**) $CaCO_3$ mass accumulation rates (MAR) at ODP Site 882 (*11*). The light gray line in (D) indicates the range in high-latitude North Atlantic, Holocene $CaCO_3$ accumulation from International ODP Site U1313 (*63*). (C and D) These data indicate that, during parts of the Pliocene, the North Pacific was both opal- and carbonate-rich, requiring that the previously noted vertical exchange supplying silicate to surface waters also included vertical mixing that reached to the seafloor at the core site (3244 m). (**E**) Focusing in on the 2.73-Ma transition, $CaCO_3$ starts to decline before the opal flux, with discrete peaks that decline in amplitude until the sediments were essentially $CaCO_3$-free. This signals a decline in the depth of winter deep convection events over a period when wintertime surface/subsurface exchange was still adequately great to import high concentrations of silicate to the surface.

extending back to 6 Ma at Site 882 indicate that even greater $CaCO_3$ burial characterized extended periods within the Pliocene (Fig. 1D). In particular, from 5.3 to 4.9 Ma and from 3.8 to 2.8 Ma, $CaCO_3$ accounted for up to 40% of the sediment. In these Pliocene intervals, nearly the entire sediment was biogenic and composed of comparable parts opal and $CaCO_3$. Whereas the opal accumulation rate was continuously high, maxima in $CaCO_3$ were sharp and orbitally paced (Fig. 1E).

The sharp, bimodal structure of $CaCO_3$ content, varying between <0.1 and 40% over multiple orbital cycles, is suggestive of preservation changes as the dominant driver just as in the Late Pleistocene (*12*). $CaCO_3$ production rate is a far less compelling explanation for the combined changes observed here, requiring large proportional production changes to generate these fluctuations, whereas the perennially high opal flux suggests high nutrient availability throughout the entire period. Moreover, coeval minima in sedimentary pigment and total organic carbon (TOC) accumulation rate provide independent evidence that the peaks in $CaCO_3$ reflect maxima in deep North Pacific ventilation (figs. S1 and S2): Between 2.8 and 3.1 Ma, pigments and TOC show a clear inverse relationship with $CaCO_3$ (figs. S1 and S2). Organic matter preservation decreases with increasing exposure time to oxygen, which rises with enhanced deep-ocean oxygen concentration (*14*). Although the sedimentary concentration and burial rate of organic matter can be influenced by various processes, such as the flux of nonbiogenic material (*15*) and total sediment burial rate, sedimentary conditions at ODP Site 882 were relatively stable during the Late Pliocene before the onset of the Northern Hemisphere glaciation at 2.73 Ma, and increased $CaCO_3$ deposition alone would have worked to raise total burial rates and thus preserve pigments and TOC during the $CaCO_3$ peaks, in the opposite sense of the observations. Accordingly, the pigment and TOC cycles are best explained as the result of elevated bottom-water oxygen during times of high $CaCO_3$ preservation. Thus, the correspondence of sharp maxima in $CaCO_3$ and minima in pigments and TOC argue strongly for periods of enhanced deep North Pacific ventilation, reaching to depths from which the signal can be mixed to the depth of the core (3244 m).

Authigenic (that is, nondetrital) uranium (U) and vanadium (V) provide complementary evidence that deep-ocean oxygen concentrations were higher before the 2.73-Ma transition (Fig. 2). The rapid accumulation of biogenic materials before this transition would have substantially enhanced respiratory oxygen demand in the sediments, tending to promote the incorporation of redox-sensitive elements, such as U and V, into the sediments (*16*). Despite this, the concentrations and accumulation rates of authigenic U and V are lower in these sediments than in the post–2.73-Ma sediments; comparison to sedimentary aluminum (Al) indicates that the U and V present in the pre–2.73-Ma sediments are nearly entirely of detrital origin (Fig. 2, A and B). This requires that the deep SNP of the warm Pliocene was characterized by high bottom-water oxygen and was therefore better ventilated than during much of the Pleistocene.

On a global basis, deep-ocean oxygen is controlled not by the rate of deep-ocean ventilation but rather by the global efficiency of the biological pump, along with the efficiency of gas exchange in polar regions (*17*, *18*). Thus, the reconstructed cycles in deep SNP $CaCO_3$ preservation state and oxygen concentration are not easily caused by ventilation changes in the North Atlantic or Southern Ocean, unless those caused major changes in the global biological pump. However, there is no evidence for large-scale biological pump changes, for example, in temperature or ice-volume cycles that would have resulted from the expected cyclic CO_2 change. In contrast, ventilation at close proximity to a deep-ocean site would be expected to cause a substantial rise

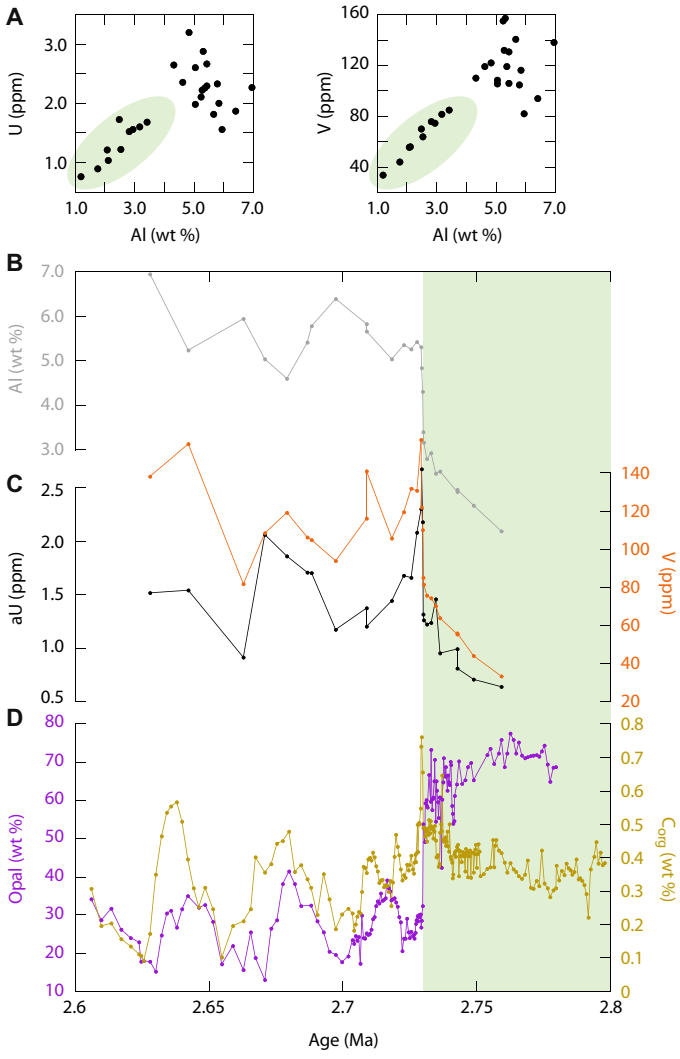

Fig. 2. Redox-sensitive trace metal records from ODP Site 882 provide complementary evidence that deep-ocean oxygen concentrations were higher before the 2.73-Ma transition. (**A**) U and V as a function of Al concentrations with values before the 2.73-Ma transition indicated by green shading. wt %, weight %. (**B**) Al, (**C**) authigenic U (aU) and V, and (**D**) opal and organic carbon (C_{org}) changes across the 2.73-Ma transition, before which U and V concentrations were low despite the export and diagenetic remineralization of organic matter being high, suggesting oxygenated conditions.

in $CaCO_3$ saturation state and oxygen concentration at that site, regardless of whether it alters the global efficiency of the biological pump for CO_2 or the solubility of CO_2 in the global ocean. Thus, the sharp, marked changes at Site 882 are best explained by intervals of convection and deep-water formation in the western SNP.

In terms of the vertical exchanges in the western SNP, the high accumulation of opal indicates that dissolved silicate from the subsurface was being imported rapidly by vertical exchange into the surface waters, fueling diatom growth. In this context, the peaks in $CaCO_3$ preservation require that this exchange sporadically reached the seafloor at Site 882. This surface-to-deep exchange would have lowered the regenerated dissolved inorganic carbon (DIC) concentration of the bottom water at Site 882 by venting excess CO_2 to the atmosphere, raising the $[CO_3^{2-}]$ and calcite saturation state of the bottom water and thus reducing dissolution

of the biogenic calcite raining to the sediments. In summary, the high opal flux indicates that (nutrient-rich) subsurface water was supplied to the surface, whereas the $CaCO_3$ preservation indicates that ventilation by surface waters reached to the deep seafloor in this region.

Pliocene elevation in $CaCO_3$ accumulation has also been observed along the California margin (*19*) and in the equatorial Pacific and Indian oceans (*20*). This increase coincides with evidence for higher organic matter fluxes to the seabed and thus higher export productivity both in low-latitude upwelling regions and at the southern margin of the central SNP (*21*). Model results suggest that the elevation in Pliocene productivity in the Pacific can be explained by the lack of an SNP halocline together with an active Pacific meridional overturning circulation (PMOC) (*22*), as discussed below. This change has been explained by an increase in vertical exchange with the onset of PMOC (*22*), an effect that would have been reinforced by higher nutrient concentrations in the SNP regions of intermediate water formation, increasing the nutrient supply to the low-latitude surface (*23*). Similarly, the apparent rise in productivity in the central SNP [for example, Sites 885 and 886; (*21*)] can be explained by convection-driven nutrient input to the surface in the western SNP, where deepest winter mixing occurs both today and in model simulations of a strong PMOC [see Fig. 3, D and E, and the study by Menviel *et al.* (*22*)], and lateral transport of the higher surface nutrients to the rest of the SNP by the subpolar gyre. However, the evidence for a productivity rise in the Indian Ocean is not easily explained by SNP changes and instead implies that the Southern Ocean overturning may have also been elevated in the Early Pliocene, as suggested previously (*10*). Further insight into the remote effects of polar overturning may arise with orbitally resolved records. Whereas halocline loss and concomitant PMOC development can explain the productivity rises in lower-latitude regions and the southern margin of the SNP, vertical nutrient supply does not limit productivity in the western SNP today, and we reiterate that TOC and pigment concentrations were lower

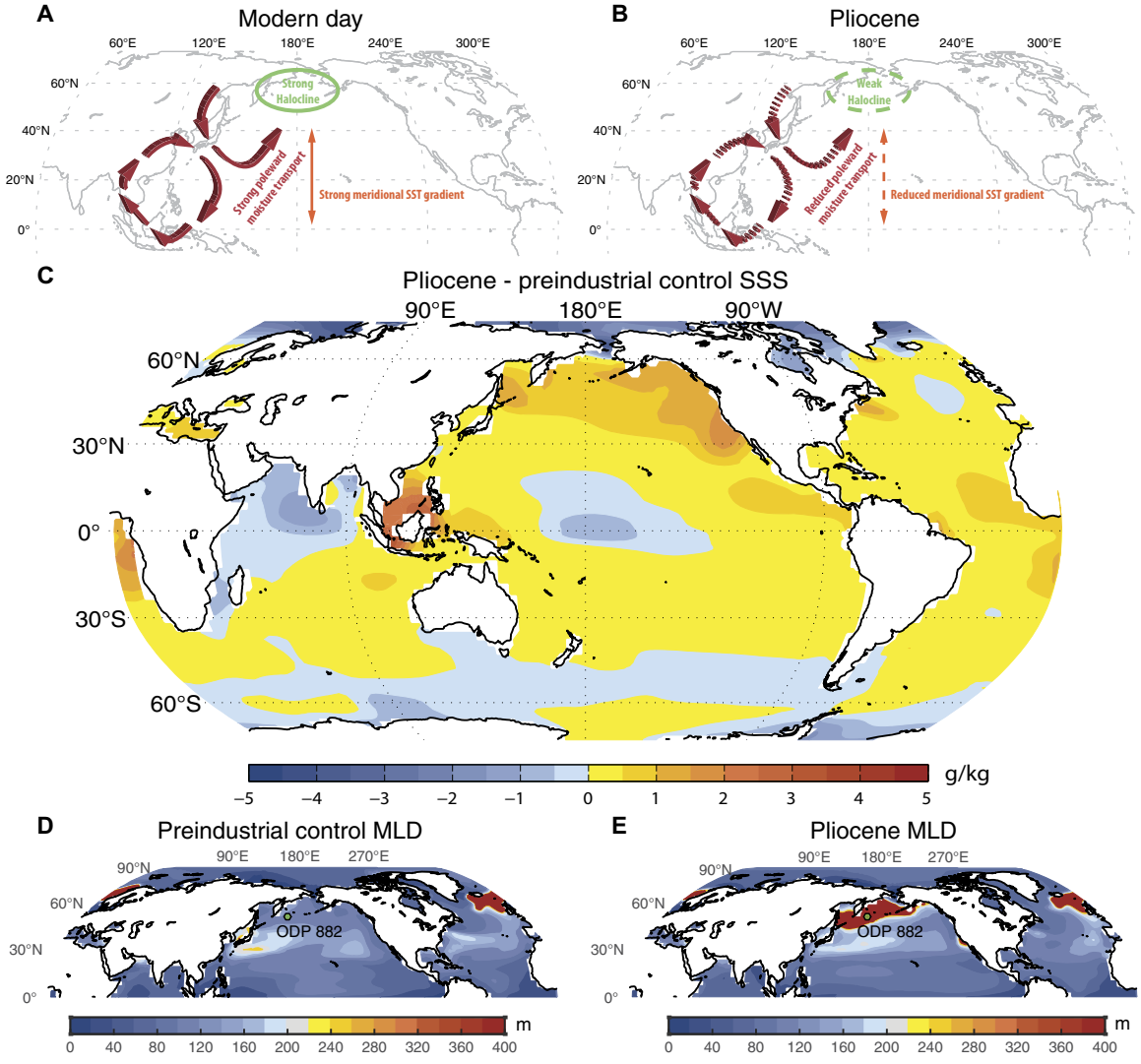

Fig. 3. NPDW formation in Pliocene simulation. (**A** and **B**) Pliocene changes in large-scale SST gradients and meridional atmospheric circulation (red arrows) support deep-water formation and ocean overturning cells in both the Atlantic and Pacific basins. (**C**) Changes in sea surface salinity (SSS) between the preindustrial and Pliocene-like simulations. (**D** and **E**) January-February-March climatological mixed-layer depths (MLD) for (D) the preindustrial control and (E) the Pliocene-like simulation. We see the appearance of substantially deeper mixed-layer depths due to winter deep-water formation in the North Pacific. ODP Site 882 (50°22′N, 167°36′E), from which the records in Figs. 1 and 2 originate, is in the region of simulated NPDW formation.

in the Pliocene $CaCO_3$ peaks of Site 882, whereas opal fluxes were effectively unchanged. Thus, the Site 882 $CaCO_3$ peaks are best explained by increases in ocean ventilation—not surface productivity—resulting from SNP convection.

In polar sediments and deep-sea sediments in general, it is extremely rare to observe high sedimentary concentrations of both opal and $CaCO_3$. Even when both biogenic components are significant, it is unusual to observe nearly equal concentrations of the two. In opal-rich sediments, such as those that occur in the Antarctic Zone of the Southern Ocean, clays and not $CaCO_3$ dominate the non-opal fraction of the sediment. In the $CaCO_3$-rich sediments of the high-latitude North Atlantic or the tropical regions in all basins, biogenic opal is scarce. The low opal content of the North Atlantic is understood as a result of the low silicate in the regional subsurface, due, in part, to the southward advection of NADW that fills much of the deep North Atlantic with low-silicate water from the surface. Although there is abundant silicate in underlying Antarctic Bottom Water, this water is not involved in the Greenland, Iceland, Norwegian, and Labrador Sea convection that produce NADW. The low-carbonate content of opal-rich Antarctic and SNP sediments has two causes. First, the high-silicate supply to the surface fuels diatom production, with coccolithophorid production being minor by comparison. Second, these regions have high-silicate supply because their subsurface waters have high concentrations of nutrients, a significant fraction of which is regenerated. Thus, in these silicate-rich regions, deep waters are high in regenerated DIC and are thus characterized by calcite undersaturation in the waters overlying the deep seafloor. Accordingly, the high-opal, high-$CaCO_3$ sediments of the Pliocene SNP require deep waters with high silicate concentration that were nevertheless adequately low in regenerated DIC to preserve substantial quantities of the $CaCO_3$ that rained to the seabed.

In the 1970s and 1980s, the contrasting opal content of North Atlantic and North Pacific sediments was linked to an estuarine circulation pattern for the modern global ocean (*24*). The North Atlantic sinking carries silicate-poor surface water into the deep ocean, and the deep water accumulates dissolved silicate from the flux of sinking matter as it flows into the Pacific. The balancing return of now silicate-rich deep water to the surface leads to the high opal flux in the North Pacific. On the basis of this paradigm, NPDW formation might have been expected to yield $CaCO_3$-rich but opal-poor sediments in the SNP, akin to those that occur in the North Atlantic.

That this is not the case helps to identify a number of important dynamics in deep-water formation that are not obvious when looking to NADW as the sole model for the process. The southward flow of NADW dominates the mid-depth chemistry of the North Atlantic basin, largely preventing silicate-rich southern-sourced water from advecting or mixing northward into the high-latitude North Atlantic. In contrast, the Pliocene NPDW formed within our simulation would not prevent silicate-rich water from flowing into the high latitudes along the eastern side of the basin. More generally, the Pacific is at zeroth-order "all" of the ocean, so it is difficult for the silicate concentration of the deep Pacific to change simply by redistributing dissolved silicate geographically through deep currents. As a result, when deep convection occurs in the North Pacific, deep water entrained in the process will import silicate to the surface, fueling the biogenic opal flux in the following summer. Thus, the high opal content of the Pliocene North Pacific sediments is consistent with SNP deep-water formation and a PMOC. Again, this is supported by the modeling results of Menviel *et al.* (*22*).

Toward the end of the Pliocene, the $CaCO_3$ decline at Site 882 started before the 2.73-Ma transition, roughly at 3 Ma, with the discrete peaks declining in amplitude until the sediments became essentially $CaCO_3$-free (Fig. 1E). In contrast, the opal flux was continuously high in the warm Pliocene, not solely during discrete events within it, and the major decline in opal flux occurred at 2.73 Ma. To raise $[CO_3^{2-}]$ and thus preserve $CaCO_3$ on the seabed at ~3000 m, deep mixing must reach to roughly that depth. In contrast, the rapid supply of dissolved silicate and the other nutrients required to sustain opal production and burial can be accomplished by vertical mixing to shallower depths in the SNP. Thus, the distinct timing of the decreases in $CaCO_3$ and opal flux through the Late Pliocene is best attributed to a shoaling of the depth to which SNP winter mixing reached. This shoaling gradually weakened and eventually prevented the discrete events of $CaCO_3$ preservation at the seafloor, whereas the final loss of vigorous winter mixing led to the opal flux drop at the 2.73-Ma transition.

What distinct features of the Pliocene would have supported NPDW formation? With the data suggesting that NPDW formation was regulated in intensity by orbital forcing and extended across most of the Pliocene, this precludes changes in ocean gateways as the primary mechanism. Furthermore, changes to the Panamanian Gateway needed to support NPDW formation are too wide and deep for the Pliocene (*25*), such that near-equilibrium simulations with imposed Miocene-Pliocene age changes in ocean gateways do not produce NPDW and a PMOC (*26*). Continuous sea surface temperature (SST) reconstructions across the past ~5 million years, covering a range of oceanic locations, reveal that the Pliocene was characterized by meridional and zonal SST gradients that were significantly weaker than observed today and since 2.73 Ma [for example, see the studies of Fedorov *et al.* (*2*, *27*)]. So far, fully coupled global climate models forced with elevated CO_2 concentrations and reconstructed mid-Piacenzian boundary conditions, without modifications in the model physics, have been unsuccessful in reproducing the full extent of reduced meridional and zonal Pliocene SST gradients [for example, see previous studies (*2*, *28*–*31*)]. Results from the Pliocene Model Intercomparison Project (PlioMIP) indicate that these models typically do not agree on the state of the Atlantic meridional overturning circulation (AMOC) during the Pliocene (*32*). None of these simulations have been shown to yield deep-water formation in the North Pacific.

Here, we demonstrate the implications of Pliocene warmth and reduced SST gradients for ocean meridional overturning in a fully coupled climate simulation that adequately reproduces Pliocene gradients and their effects on atmospheric circulation. Given sensitivity experiments and theoretical considerations (*2*, *27*, *33*), a change in the equator-to-pole, top-of-the-atmosphere energy budget is required to maintain the structurally different global surface and subsurface temperature fields of the Pliocene, including the reduced meridional SST gradient [Fig. 4; see also the study by Burls and Fedorov (*34*)]. See Materials and Methods for a discussion of the relative influence of the mechanisms proposed in the literature and the model modifications imposed in this study (affecting cloud albedo) that alter the top-of-the-atmosphere radiation budget, allowing for a sufficient reduction in the meridional SST gradient as the coupled system freely adjusts to the changes in radiative forcing. We stress that this simulation was chosen from a range of sensitivity experiments purely because of the good agreement with reconstructed Pliocene SSTs [see the study by Burls and Fedorov (*34*)] and was in no way tuned to produce NPDW formation—this was instead a serendipitous outcome in the equilibrium state of the simulation (see fig. S3).

Initially, during the model spin-up, in response to the imposed mid- and high-latitude ocean surface warming, and the associated increase in subarctic upper-ocean stratification, the AMOC decreases substantially (fig. S3). However, as the Pliocene-like simulation is run toward equilibrium, heat slowly diffuses down into the deep ocean, and the AMOC recovers but still remains ~30% weaker than the control simulation (figs. S3 and S4). Concurrently, after some 1500 years of simulation, a strong meridional overturning circulation develops in the Pacific basin (fig. S3), with deep water forming in the Bering Sea (Fig. 3E). The decreased AMOC strength within our simulation could, to some extent,

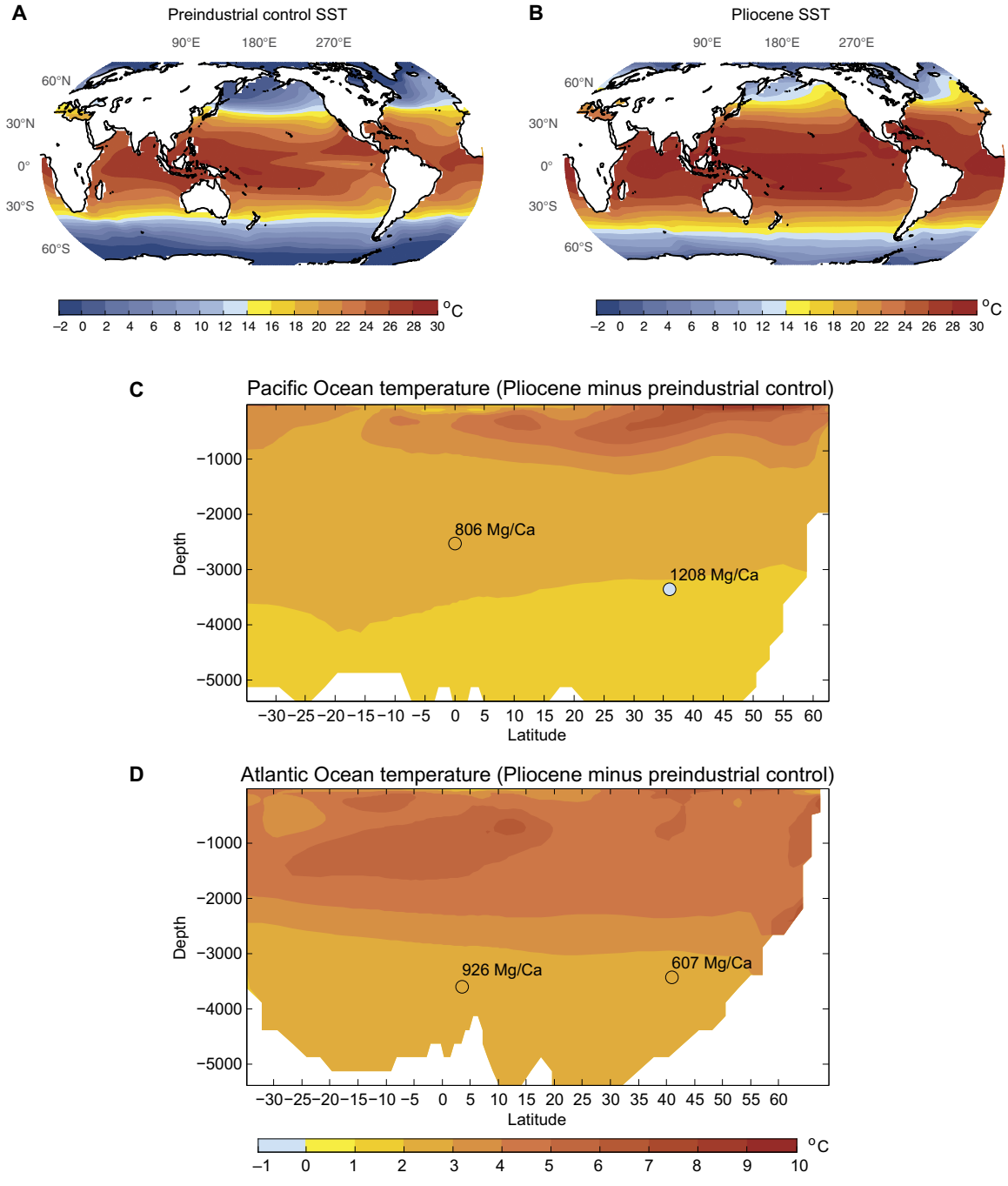

Fig. 4. Weak SST gradients and subsurface warming in Pliocene simulation. Annual mean SSTs for (**A**) the preindustrial control and (**B**) the Pliocene-like experiment. Note the reduced meridional and zonal large-scale SST gradients within the Pliocene-like simulation [see the study by Burls and Fedorov (*34*) for a detailed comparison with available SST reconstructions from locations around the globe]. (**C** and **D**) Zonal-mean ocean temperature change between the Pliocene-like and control simulations for (C) the Pacific and (D) the Atlantic. Superimposed circles show estimated Pliocene temperature changes based on available reconstructions. Consistent with North Atlantic temperature reconstructions from Site 607 (*36*) and Site 926 (*37*), the deep ocean is 2° to 3°C warmer in Pliocene simulation. In line with the estimates by Lear *et al.* (*37*) from Site 806, waters between 2000 and 3000 m in the Pacific are 2° to 3°C warmer. Below 3000 m, the deep-ocean warming is less in the Pacific Ocean than in the Atlantic, with bottom-water temperatures only between 1° and 2°C warmer than the control, which is arguably consistent with recent Pliocene bottom-water temperature estimates (*40*).

contribute to the development of the PMOC circulation via the Atlantic-Pacific seesaw mechanism (*6*). However, as described below, changes in the surface buoyancy forcing, particularly changes in surface evaporation and precipitation fields as part of the hydrological cycle, act directly within each basin to drive the concurrent changes in deep-water formation.

The equilibrium AMOC change between the Pliocene-like and preindustrial experiments (fig. S4) is related to the changes in the thermal stratification within the subarctic North Atlantic. In particular, a 4° to 9°C warming of the upper ocean (with a maximum zonal mean SST change of 6° to 7°C between 40° and 50°N) is accompanied by only a 2° to 3°C warming in bottom-water temperatures (Fig. 4). The simulated surface warming is consistent with SST reconstructions, for instance, from Site 607 (*35*) [for a comprehensive model-observation comparison, see Fig. 3 and Table 2 of Burls and Fedorov's work (*34*)]. Likewise, the increase in deep-ocean temperature is in line with reconstructions from Site 607 (*36*) and Site 926 (*37*), as shown in Fig. 4C. This enhanced upper-ocean warming acts to increase the thermal stratification in the mid- to high-latitude Northern Atlantic relative to the preindustrial control simulation, weakening deep-water formation and the AMOC.

Similarly, in the northern Pacific, a 4° to 9°C warming of the upper ocean (with a maximum zonal mean SST change of 7° to 8°C between 40°N and 50°N) is accompanied by only a 1° to 2°C warming in bottom-water temperatures (Fig. 4). The simulated midlatitude surface warming is consistent with SST reconstructions from Site 1208 (*38*, *39*) and Site 1021 (*39*). Specifically, for the SNP, it is worth noting that the pre-industrial control simulation has a substantial cold SST bias relative to the present-day SSTs. As a result, the surface and upper-ocean warming at Site 882 within the Pliocene experiment is reduced relative to the observed present-day (WOA09) ocean temperatures (fig. S6A). As shown in Fig. 4D, the simulated deep-ocean warming in the Pacific generally agrees with reconstructions from Site 806 (*37*) and (to a lesser extent) Site 1208 (*40*), with the deep North Pacific warming less than the deep North Atlantic.

If the enhanced surface warming in the SNP occurred in isolation, it would act to increase ocean stratification at Site 882. However, it is overcome by a substantial increase in surface salinity (1 to 2 practical salinity units; Fig. 3C), which erodes the northern Pacific halocline (figs. S5A and S6B). The net result is decreased SNP density stratification and deep-water formation during the winter months when surface SSTs cool (fig. S6), giving rise to deep-water formation in this region (Fig. 3E and fig. S6C) and the development of a PMOC (Fig. 5) cell of nearly 17 Sv.

Increased North Pacific surface water salinity within our Pliocene-like experiment is the result of changes in atmospheric hydrological forcing driven by the reduced meridional SST gradients within this coupled experiment (Fig. 3 and figs. S7 and S8A). In the zonal mean, weakening of the Hadley circulation and of the subtropical high-pressure systems due to the reduced meridional SST gradients results

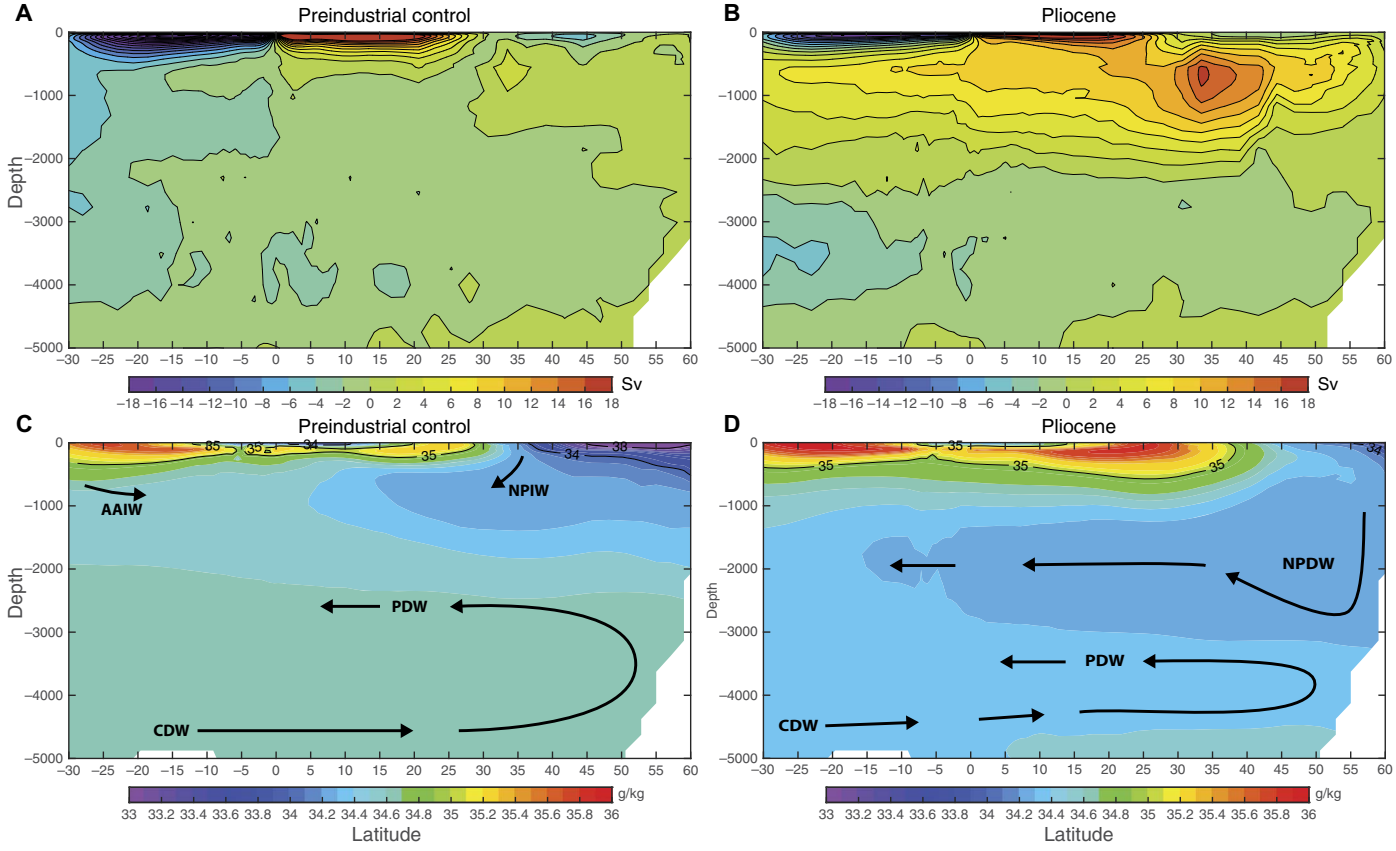

Fig. 5. PMOC and NPDW formation in Pliocene simulation. Indo-Pacific zonal-mean stream functions for (**A**) the preindustrial control and (**B**) the Pliocene-like simulation. The adjusted oceanic state within our simulation with a Pliocene-like SST pattern supports meridional overturning in the Pacific basin. Zonal-mean Pacific salinity for (**C**) the preindustrial control and (**D**) the Pliocene-like simulation shows NPDW (fresher than other deep waters) forming in the SNP and filling the North Pacific between ~1000 and 3000 m. AAIW, Antarctic Intermediate Water; NPIW, North Pacific Intermediate Water; PDW, Pacific Deep Water; CDW, Circumpolar Deep Water.

in reduced moisture flux divergence in the subtropics and convergence in the tropics and midlatitudes. These moisture flux changes reduce precipitation minus evaporation ($P - E$) in the tropics (10°S to 10°N) and midlatitudes (30° to 55°N and S) and increase it in the subtropics (10° to 30°N and S) and high latitudes (55° to 90°N and S). Reduced subtropical and high-latitude moisture divergence acts to increase precipitation over the subtropical North Pacific while reducing precipitation over the tropical and midlatitude North Pacific (fig. S7). Figure S8A illustrates the effect of these changes on atmospheric freshwater forcing over the subtropical and subarctic ocean gyres.

To further diagnose the physical processes supporting higher upper-ocean (0 to 200 m) salinities within the Pacific subpolar gyre, a salinity budget (table S2 and fig. S8B), following the approach of Warren (*3*) and Emile-Geay (*5*), has been assessed for not only the subpolar gyre (43.1°N to 65.8°N) but also the northern midlatitude extent of the subtropical gyre (27.4°N to 43.1°N). These salt budgets reveal that the changes in the atmospheric freshwater flux influence the salinity of the subpolar gyre primarily through changes in the salinity of midlatitude waters advected and upwelled into the subpolar gyre (see fig. S8B and the Supplementary Text).

The corresponding increase in mid- to high-latitude upper-ocean salinity is weaker in the Atlantic (Fig. 3C and fig. S5B)—the decrease in midlatitude $P - E$ in the Pliocene-like simulation is somewhat weaker over the Atlantic and is counteracted by an oceanic freshwater flux from the Arctic, which receives enhanced $P - E$ due to increased atmospheric moisture convergence in the high latitudes (fig. S7). The fresher Arctic waters flow more freely into the North Atlantic than the Pacific, counteracting the effects of decreased midlatitude $P - E$ over

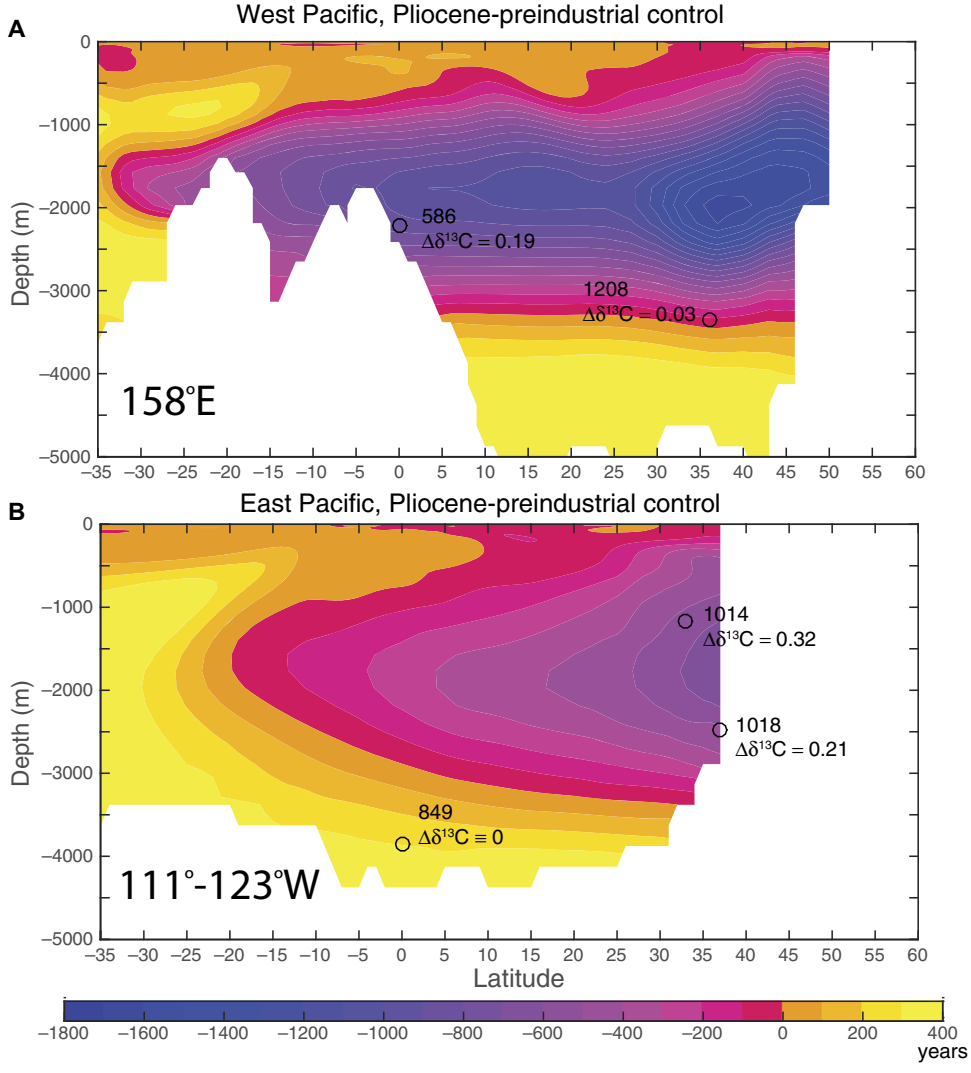

Fig. 6. Simulated North Pacific ventilation changes versus observed Pliocene $\delta^{13}C$ differences from the Late Pleistocene interglacial values. Pliocene-control changes in ventilation age along (**A**) 158°E (the longitude of ODP Sites 586 and 1208) and (**B**) the average between 111° and 123°W (the longitude range of ODP Sites 849, 1014, and 1018). Superimposed circles show Pliocene $\delta^{13}C$ differences from Late Pleistocene interglacial values for Sites 586, 849, 1014, and 1018 [see Table 2 of Ravelo and Andreasen (*47*)] and for Site 2018 [(*40*); using the same approach as by Ravelo and Andreasen (*47*) for the 1208 record, with average Holocene values serving as the Late Pleistocene estimate, and 3.1- to 3.37-Ma values as the Pliocene estimate, and with Site 849 used to correct for global ocean $\delta^{13}C$ changes]. Note that whereas the PMOC results in varying degrees of enhanced North Pacific ventilation for all depths above ~3500 m, the presence of a deep western boundary current (see fig. S15) leads to increased ventilation in the western Pacific, thus accounting for the higher Pliocene $\delta^{13}C$ observed at Site 586.

the North Atlantic to a much greater extent than in the Pacific. The net effect of these SST and salinity changes on the surface density field is shown in fig. S9. Increased upper-ocean salinities in the subarctic Pacific increase the meridional density gradient despite reduced meridional temperature gradients. Because of the stronger Arctic influence, comparable upper-ocean salinity changes do not occur in the high-latitude northern Atlantic, such that the AMOC weakens, but only by ~30% (figs. S3 and S4). The resulting global ocean state, in contrast to the modern ocean, has deep-water formation in both the North Atlantic and the North Pacific.

Whereas these changes in the surface freshwater forcing of the North Pacific are primarily responsible for the disappearance of the halocline and the strengthened subpolar gyre meridional density gradient within the Pliocene simulation, a secondary factor contributing to the presence of NPDW formation within the Pliocene simulation is the effect of the mean ocean warming. By virtue of the nonlinear equation of state of seawater, mean ocean warming tends to increase the meridional density gradient and promote deep-water formation (fig. S10) (*10*, *41*).

Whereas we see some weakening of the AMOC concurrent with the PMOC activation, the combined global overturning is elevated in our Pliocene experiment. de Boer *et al.* (*41*) found a similar result, with global deep ventilation increasing with dynamical warming across their simulations. The net upward volume transport of Northern Hemisphere–sourced waters in the Southern Ocean (driven by winds) remains similar between our Pliocene and the control experiments (~12 Sv), but upward transport through the equatorial thermocline is enhanced within the Indo-Pacific (Fig. 5). This enhanced transport across the thermocline appears to be consistent with the modified diffusive scaling in the presence of wind-driven gyres discussed by Vallis [(*42*), p. 673] as in the Pacific the effect of the gyre circulation is felt as deep as 800 m and deeper (fig. S11). In the Pliocene experiment, vertical stratification in the upper ~200 to 300 m of the shallow subtropical cells is reduced in both basins relative to the control (fig. S12), which is due to reduced meridional gradients in temperature (Fig. 4B) and hence density (fig. S9) within the subtropical gyres. At the same time, in accordance with the two-thermocline limit theory (*43*), the increased surface meridional density gradient due to salinity changes in the North Pacific subpolar gyre results in increased static stability between ~300 and 1000 m (figs. S9 and S12).

With the exception of the upper 100 m and the convecting subarctic Pacific, vertical diffusivity is similar between the Pliocene and control (figs. S13 and S14). The input of mechanical energy by winds and tides required to upwell cold water from the deep ocean places a constraint on the global overturning circulation (*44*). The energy used by background and tidal vertical mixing is a diagnostic variable of the ocean model component, and, assuming a mixing efficiency of 0.2 (*45*), the globally averaged power consumed by this vertical mixing is estimated as 1.74 TW in the control and 1.68 TW in the Pliocene experiment [the K-profile parameterization vertical mixing scheme was used in the Parallel Ocean Program 2 (POP2) ocean component]. This slight reduction in the energy used by mixing in the Pliocene experiment is consistent with similar values of vertical diffusivities but somewhat weaker surface winds in this simulation.

Simulated changes in water ventilation age for an active PMOC broadly agree with benthic foraminiferal carbon isotope ($\delta^{13}C$) data from available North Pacific sites (Fig. 6), suggesting enhanced Pliocene ventilation above 3500 m (*46*, *47*). Whereas Kwiek and Ravelo (*46*) and Ravelo and Andreasen (*47*) proposed enhanced North Pacific intermediate water formation during the Pliocene to explain their $\delta^{13}C$ results, our simulation illustrates that NPDW formation and the associated PMOC are required to ventilate the North Pacific to the extent suggested by these records.

It would appear that ODP Site 882 is ideally located to detect the North Pacific winter deep-water formation because it sits within the region of simulated winter mixed-layer deepening (Fig. 3E). Furthermore, within the Pliocene-like simulation, considerable internal variability is seen in the strength of the PMOC and depth of North Pacific winter deep-water formation (figs. S3 and S16) that would have been further amplified by orbitally driven fluctuations in Pliocene meridional SST gradients, consistent with the orbitally paced variability in $CaCO_3$ accumulation at Site 882. Together, the $CaCO_3$ and redox-sensitive trace metal data from ODP Site 882, the simulated response to Pliocene SST gradients, and the North Pacific $\delta^{13}C$ data present a strong argument for Pliocene SNP deep-water formation that penetrated into the North Pacific between ~1000 and 3500 m (Fig. 5) and experienced an orbital pacing in intensity and depth of convection.

DISCUSSION

It is generally expected that the SNP will develop stronger density stratification under global warming due to both a more rapid warming of the upper relative to the deep ocean and an intensification of the hydrological cycle that freshens high-latitude regions (*48*). However, insofar as the warm Pliocene is an appropriate analog, our findings suggest that this effect could be transient and that the long-term outcome of global warming may be roughly the opposite: reduced density stratification of the SNP and increased communication with the deep ocean. If so, the role of deep-ocean circulation in Northern Hemisphere heat transport (for example, figs. S17 and S18) and the global ocean's ecosystems would be thoroughly transformed.

MATERIALS AND METHODS

Paleoceanographic measurements

The carbonate ($CaCO_3$) contents of ODP Site 882 were determined by coulometric analyses using a Coulomat 702 at Kiel University (*11*). The accuracy was better than 2%, as obtained by replicate and standard measurements. TOC concentrations were determined by subtracting $CaCO_3$ from total carbon concentrations determined by combustion. Sedimentary pigments were analyzed at the Biogeochemistry Centre of Bristol University using a Philips UV/VIS spectrophotometer at wavelengths of 410 nm after extraction with 3:1 dichloromethane/methanol. Absolute elemental concentrations were measured by inductively coupled plasma mass spectrometry (ELAN 5000A) using solution nebulization after mixed-acid digestion ($HF\text{-}HCLO_4$) under pressure. Precision and accuracy were better than 5%. The authigenic fraction of U was estimated by normalization to Al; $aU = U_{mes} - (U/Al_{BCC} \times Al)$, with $U/Al_{BCC} = 1.08 \times 10^{-5}$ (*49*). The calculations of aU are based on the assumption that the composition of the Al phases of the terrigenous material remained constant in space and time and are well represented by the bulk continental crust (BCC) end member.

Pliocene simulation

Our numerical simulations were performed using the Community Earth System Model (CESM) version 1.0.4, developed by the National Center for Atmospheric Research. We used the T31 gx3v7 configuration (*50*), designed for performing long paleoclimate simulations, wherein the atmospheric and land surface components (Community Atmosphere Model 4 and Community Land Model) have a spectral truncation of

T31, and the oceanic and sea ice (POP2 and Community Ice Code) components have a resolution varying from 3° near the poles to 1° at the equator. This model was further modified using the approach of Burls and Fedorov (*33*), who explored the sensitivity of large-scale SST gradients to the meridional gradient in cloud radiative forcing by changing the reflectivity of clouds as they formed within CESM. As the most straightforward way of changing cloud albedo, the atmospheric liquid and ice water paths were scaled within targeted latitudinal band, but only in the shortwave radiation scheme.

Building on these results, the magnitude and spatial structure of the latitudinal cloud albedo changes needed to reproduce the large-scale features within a global reconstruction of Early Pliocene surface and subsurface temperatures were established by Burls and Fedorov (*34*) [Fig. 4; see also Fedorov *et al.* (*27*) for further comparison with large-scale meridional SST gradients]. By reducing the liquid water path (that is, low liquid clouds and not high ice clouds) poleward of 15°N and S, the reflectivity of low-level extratropical clouds and, as a result, mean cloud albedo is reduced in the extratropics (8° to 90°N and S) by 0.04 relative to the preindustrial control configuration. In the tropics, both the liquid and ice paths were increased, thereby increasing the albedo of both low and high clouds and mean tropical albedo (8°S to 8°N) by 0.06. All the other elements of the climate system, as simulated within CESM, remained unaltered and were allowed to freely evolve as the oceanic and atmospheric components adjusted to the imposed changes in cloud shortwave radiative forcing. This coupled ocean atmosphere simulation, which achieves a good agreement with the available proxy SST data for the Pliocene in both low and high latitudes (*34*), is referred to here as the Pliocene-like simulation and is compared to the standard preindustrial control simulation.

The ultimate goal of the modifications to cloud physics is to reproduce the observed reduction in the meridional SST gradient evident in the proxy data for the Pliocene [for example, see previous studies (*2*, *27*, *30*, *31*)]. The weakening of the meridional gradients translates into a reduction of the zonal SST gradient along the equator. As highlighted in the study by Fedorov *et al.* (*27*) and corroborated by the PlioMIP results, the response of large-scale SST gradients in climate models to reconstructed Pliocene CO_2 forcing (~400 ppm) is too weak, and unreasonably large changes in CO_2 and hence global mean temperature are required to reduce the meridional gradient to Pliocene values. This points to poorly or unresolved processes within these models, with clouds as one of the strongest sources of uncertainty (*51*). Although changes in ocean gateways [for example, see previous studies (*52*–*55*)], such as an open Central American Seaway or a more southerly position of Indonesia, are possible contributors, their effects tend to be somewhat regional and are not sufficient to support the large-scale SST patterns during the Pliocene (*2*, *26*, *55*). Likewise, the simulated effects of possible changes in orography tend to be fairly regional, and as with ocean gateways, their timing is hard to confine (*56*–*58*).

Theoretical considerations (*27*, *33*, *59*) highlight that the large-scale weakening of meridional SST gradients during the Pliocene would have been associated with significantly reduced off-equatorial wind-driven ocean heat transport. To the extent that the partitioning of the meridional heat transport between the atmospheric and oceanic components should remain approximately constant (*60*), a change in the top-of-the-atmosphere energy budget is required to maintain the reduced ocean heat transport and SST gradients of the Pliocene [Fig. 4; see also the study by Burls and Fedorov (*34*)]. The required change in the meridional structure of net cloud radiative forcing during the Pliocene could have occurred via shortwave, longwave, or both, realized by changes in a number of cloud properties in addition to liquid and ice water content (for example, cloud lifetime and particle concentration and size) and sustained by different Pliocene atmospheric aerosol concentrations [for example, see the study by Unger and Yue (*61*)] or unresolved cloud feedbacks to elevated CO_2 levels during the Pliocene (*34*).

Further, when studying changes in deep-water formation and ocean meridional overturning circulation, it is essential to ensure that the deep ocean has fully adjusted, and as such, our Pliocene-like simulation has been run for 3000 years, allowing the simulation to reach near-equilibrium. The analysis presented here is based on the last 500 years of the Pliocene and control simulations, when the top-of-the-atmosphere imbalance reaches only 0.02 and −0.04 W m^{-2} for the two respective simulations. It is noteworthy that the PMOC becomes fully established only after some 1500 years of computation (fig. S3).

SUPPLEMENTARY MATERIALS

Supplementary material for this article is available at http://advances.sciencemag.org/cgi/content/full/3/9/e1700156/DC1

Supplementary Text

fig. S1. Deep-ocean ventilation as the driver of $CaCO_3$ cycles.

fig. S2. Pliocene variations in porphyrin and TOC concentrations at Site 882.

fig. S3. Oceanic adjustment and the development of a PMOC.

fig. S4. Atlantic zonal-mean stream functions.

fig. S5. Simulated changes in ocean salinity.

fig. S6. Simulated and observed temperature, salinity, and density profiles at Site 882.

fig. S7. Simulated precipitation minus evaporation changes.

fig. S8. Atmospheric moisture transport and oceanic salinity budget.

fig. S9. Simulated surface density change between the preindustrial and Pliocene-like experiments.

fig. S10. Simulated January-February-March potential density profiles at the approximate location of Site 882.

fig. S11. Vertical velocities across ~800 m.

fig. S12. Simulated changes in ocean static stability.

fig. S13. Zonal mean Pacific vertical diffusivity (cm^2/s).

fig. S14. Vertical diffusivity at ~800 m.

fig. S15. Change in North Pacific deep-ocean (1000 to 2000 m) currents between the Pliocene and preindustrial control experiments.

fig. S16. Variability in the PMOC.

fig. S17. Simulated zonal mean meridional heat transport.

fig. S18. Simulated surface currents and theoretical wind-driven Sverdrup flow.

table S1. List of the salt budget variables.

table S2. The contribution of the change in each variable, $\delta\zeta_i$, to the change in salinity, $\Sigma_i\Delta_{\zeta i}$, of the Subarctic and midlatitude regions between the control and Pliocene simulations, as shown in fig. S8B.

Reference (*64*)

REFERENCES AND NOTES

1. M. A. Martínez-Botí, G. L. Foster, T. B. Chalk, E. J. Rohling, P. F. Sexton, D. J. Lunt, R. D. Pancost, M. P. S. Badger, D. N. Schmidt, Plio-Pleistocene climate sensitivity evaluated using high-resolution CO_2 records. *Nature* **518**, 49–54 (2015).
2. A. V. Fedorov, C. M. Brierley, K. T. Lawrence, Z. Liu, P. S. Dekens, A. C. Ravelo, Patterns and mechanisms of early Pliocene warmth. *Nature* **496**, 43–49 (2013).
3. B. A. Warren, Why is no deep water formed in the North Pacific? *J. Mar. Res.* **41**, 327–347 (1983).
4. T. F. Stocker, D. G. Wright, Rapid transitions of the ocean's deep circulation induced by changes in surface water fluxes. *Nature* **351**, 729–732 (1991).
5. J. Emile-Geay, M. A. Cane, N. Naik, R. Seager, A. C. Clement, A. van Geen, Warren revisited: Atmospheric freshwater fluxes and "Why is no deep water formed in the North Pacific." *J. Geophys. Res. Atmos.* **108**, 3178–3112 (2003).
6. O. A. Saenko, A. Schmittner, A. J. Weaver, The Atlantic–Pacific seesaw. *J. Climate* **17**, 2033–2038 (2004).
7. D. Ferreira, J. Marshall, J.-M. Campin, Localization of deep water formation: Role of atmospheric moisture transport and geometrical constraints on ocean circulation. *J. Climate* **23**, 1456–1476 (2010).

8. G. H. Haug, D. M. Sigman, R. Tiedemann, T. F. Pedersen, M. Sarnthein, Onset of permanent stratification in the subarctic Pacific Ocean. *Nature* **401**, 779–782 (1999).
9. A. S. Studer, A. Martínez-Garcia, S. L. Jaccard, F. E. Girault, D. M. Sigman, G. H. Haug, Enhanced stratification and seasonality in the Subarctic Pacific upon Northern Hemisphere Glaciation—New evidence from diatom-bound nitrogen isotopes, alkenones and archaeal tetraethers. *Earth Planet. Sci. Lett.* **351–352**, 84–94 (2012).
10. D. M. Sigman, S. L. Jaccard, G. H. Haug, Polar ocean stratification in a cold climate. *Nature* **428**, 59–63 (2004).
11. G. H. Haug, M. A. Maslin, M. Sarnthein, R. Stax, R. Tiedemann, in *Proceedings of the Ocean Drilling Program, Scientific Results*, vol. 145, D. K. Rea, I. A. Basov, D. W. Scholl, J. F. Allan, Eds. (Ocean Drilling Program, 1995), pp. 293–314.
12. S. L. Jaccard, S. L. Jaccard, G. H. Haug, D. M. Sigman, T. F. Pedersen, H. R. Thierstein, U. Röhl, Glacial/interglacial changes in Subarctic North Pacific stratification. *Science* **308**, 1003–1006 (2005).
13. E. D. Galbraith, S. L. Jaccard, T. F. Pedersen, D. M. Sigman, G. H. Haug, M. Cook, J. R. Southon, R. Francois, Carbon dioxide release from the North Pacific abyss during the last deglaciation. *Nature* **449**, 890–893 (2007).
14. H. E. Hartnett, R. G. Keil, J. I. Hedges, A. H. Devol, Influence of oxygen exposure time on organic carbon preservation in continental margin sediments. *Nature* **391**, 572–575 (1998).
15. K. A. F. Zonneveld, G. J. M. Versteegh, S. Kasten, T. I. Eglinton, K.-C. Emeis, C. Huguet, B. P. Koch, G. J. de Lange, J. W. de Leeuw, J. J. Middelburg, G. Mollenhauer, F. G. Prahl, J. Rethemeyer, S. G. Wakeham, Selective preservation of organic matter in marine environments; processes and impact on the sedimentary record. *Biogeosciences* **7**, 483–511 (2010).
16. N. Tribovillard, T. J. Algeo, T. Lyons, A. Riboulleau, Trace metals as paleoredox and paleoproductivity proxies: An update. *Chem. Geol.* **232**, 12–32 (2006).
17. D. M. Sigman, M. P. Hain, G. H. Haug, The polar ocean and glacial cycles in atmospheric CO_2 concentration. *Nature* **466**, 47–55 (2010).
18. S. Jaccard, E. D. Galbraith, T. L. Frölicher, N. Gruber, Ocean (de)oxygenation across the last deglaciation: Insights for the future. *Oceanography* **27**, 26–35 (2014).
19. A. C. Ravelo, M. Lyle, I. Koizumi, J. P. Caulet, E. Fornaciari, A. Hayashida, F. Heider, J. Hood, S. Hovan, T. Janecek, A. Janik, R. Stax, Pliocene carbonate accumulation along the California Margin. *Paleoceanography* **12**, 729–741 (1997).
20. G. R. Dickens, R. M. Owen, The Latest Miocene–Early Pliocene biogenic bloom: A revised Indian Ocean perspective. *Mar. Geol.* **161**, 75–91 (1999).
21. G. R. Dickens, R. M. Owen, Sediment geochemical evidence for an early-middle Gilbert (early Pliocene) productivity peak in the North Pacific Red Clay Province. *Mar. Micropaleontol.* **27**, 107–120 (1996).
22. L. Menviel, A. Timmermann, O. E. Timm, A. Mouchet, A. Abe-Ouchi, M. O. Chikamoto, N. Harada, R. Ohgaito, Y. Okazaki, Removing the North Pacific halocline: Effects on global climate, ocean circulation and the carbon cycle. *Deep-Sea Res. II Top. Stud. Oceanogr.* **61–64**, 106–113 (2012).
23. J. L. Sarmiento, N. Gruber, M. A. Brzezinski, J. P. Dunne, High-latitude controls of thermocline nutrients and low latitude biological productivity. *Nature* **427**, 56–60 (2004).
24. W. H. Berger, Biogenous deep-sea sediments: Fractionation by deep-sea circulation. *Geol. Soc. Am. Bull.* **81**, 1385–1402 (1970).
25. T. Motoi, W.-L. Chan, S. Minobe, H. Sumata, North Pacific halocline and cold climate induced by Panamanian Gateway closure in a coupled ocean-atmosphere GCM. *Geophys. Res. Lett.* **32**, L10618 (2005).
26. C. M. Brierley, A. V. Fedorov, Comparing the impacts of Miocene–Pliocene changes in inter-ocean gateways on climate: Central American Seaway, Bering Strait, and Indonesia. *Earth Planet. Sci. Lett.* **444**, 116–130 (2016).
27. A. V. Fedorov, N. J. Burls, K. T. Lawrence, L. C. Peterson, Tightly linked zonal and meridional sea surface temperature gradients over the past five million years. *Nat. Geosci.* **8**, 975–980 (2015).
28. A. M. Haywood, P. J. Valdes, V. L. Peck, A permanent El Niño–like state during the Pliocene? *Paleoceanography* **22**, PA1213 (2007).
29. D. J. Lunt, A. M. Haywood, G. A. Schmidt, U. Salzmann, P. J. Valdes, H. J. Dowsett, Earth system sensitivity inferred from Pliocene modelling and data. *Nat. Geosci.* **3**, 60–64 (2009).
30. H. J. Dowsett, K. M. Foley, D. K. Stoll, M. A. Chandler, L. E. Sohl, M. Bentsen, B. L. Otto-Bliesner, F. J. Bragg, W.-L. Chan, C. Contoux, A. M. Dolan, A. M. Haywood, J. A. Jonas, A. Jost, Y. Kamae, G. Lohmann, D. J. Lunt, K. H. Nisancioglu, A. Abe-Ouchi, G. Ramstein, C. R. Riesselman, M. M. Robinson, N. A. Rosenbloom, U. Salzmann, C. Stepanek, S. L. Strother, H. Ueda, Q. Yan, Z. Zhang, Sea surface temperature of the mid-piacenzian ocean: A data-model comparison. *Sci. Rep.* **3**, 2013 (2013).
31. C. Brierley, N. Burls, C. Ravelo, A. Fedorov, Pliocene warmth and gradients. *Nat. Geosci.* **8**, 419–420 (2015).
32. Z.-S. Zhang, K. H. Nisancioglu, M. A. Chandler, A. M. Haywood, B. L. Otto-Bliesner, G. Ramstein, C. Stepanek, A. Abe-Ouchi, W.-L. Chan, F. J. Bragg, C. Contoux, A. M. Dolan, D. J. Hill, A. Jost, Y. Kamae, G. Lohmann, D. J. Lunt, N. A. Rosenbloom, L. E. Sohl, H. Ueda, Mid-pliocene Atlantic meridional overturning circulation not unlike modern? *Clim. Past Discuss.* **9**, 1297–1319 (2013).
33. N. J. Burls, A. V. Fedorov, What controls the mean east–west sea surface temperature gradient in the equatorial Pacific: The role of cloud albedo. *J. Climate* **27**, 2757–2778 (2014).
34. N. J. Burls, A. V. Fedorov, Simulating Pliocene warmth and a permanent El Niño-like state: The role of cloud albedo. *Paleoceanography* **29**, 893–910 (2014).
35. K. T. Lawrence, S. Sosdian, H. E. White, Y. Rosenthal, North Atlantic climate evolution through the Plio-Pleistocene climate transitions. *Earth Planet. Sci. Lett.* **300**, 329–342 (2010).
36. S. Sosdian, Y. Rosenthal, Deep-sea temperature and ice volume changes across the Pliocene-Pleistocene climate transitions. *Science* **325**, 306–310 (2009).
37. C. H. Lear, Y. Rosenthal, J. D. Wright, The closing of a seaway: Ocean water masses and global climate change. *Earth Planet. Sci. Lett.* **210**, 425–436 (2003).
38. M. Pagani, Z. Liu, J. LaRiviere, A. C. Ravelo, High Earth-system climate sensitivity determined from Pliocene carbon dioxide concentrations. *Nat. Geosci.* **3**, 27–30 (2009).
39. J. P. LaRiviere, A. C. Ravelo, A. Crimmins, P. S. Dekens, H. L. Ford, M. Lyle, M. W. Wara, Late Miocene decoupling of oceanic warmth and atmospheric carbon dioxide forcing. *Nature* **486**, 97–100 (2012).
40. S. C. Woodard, Y. Rosenthal, K. G. Miller, J. D. Wright, B. K. Chiu, K. T. Lawrence, Antarctic role in Northern Hemisphere glaciation. *Science* **346**, 847–851 (2014).
41. A. M. de Boer, D. M. Sigman, J. R. Toggweiler, J. L. Russell, Effect of global ocean temperature change on deep ocean ventilation. *Paleoceanography* **22**, PA2210 (2007).
42. G. K. Vallis, *Atmospheric and Oceanic Fluid Dynamics: Fundamentals and Large-Scale Circulation* (Cambridge Univ. Press, 2006).
43. R. M. Samelson, G. K. Vallis, Large-scale circulation with small diapycnal diffusion: The two-thermocline limit. *J. Mar. Res.* **55**, 223–275 (1997).
44. C. Wunsch, R. Ferrari, Vertical mixing, energy, and the general circulation of the oceans. *Annu. Rev. Fluid Mech.* **36**, 281–314 (2004).
45. L. S. Laurent, H. Simmons, Estimates of power consumed by mixing in the ocean interior. *J. Climate* **19**, 4877–4890 (2006).
46. P. B. Kwiek, A. C. Ravelo, Pacific Ocean intermediate and deep water circulation during the Pliocene. *Palaeogeogr. Palaeoclimatol. Palaeoecol.* **154**, 191–217 (1999).
47. A. C. Ravelo, D. H. Andreasen, Enhanced circulation during a warm period. *Paleoceanography* **27**, 1001–1004 (2000).
48. J. L. Sarmiento, T. M. C. Hughes, R. J. Stouffer, S. Manabe, Simulated response of the ocean carbon cycle to anthropogenic climate warming. *Nature* **393**, 245–249 (1998).
49. S. R. Taylor, S. M. McLennan, The geochemical evolution of the continental crust. *Rev. Geophys.* **33**, 241–265 (1995).
50. C. A. Shields, D. A. Bailey, G. Danabasoglu, M. Jochum, J. T. Kiehl, S. Levis, S. Park, The low-resolution CCSM4. *J. Climate* **25**, 3993–4014 (2012).
51. D. J. Hill, A. M. Haywood, D. J. Lunt, S. J. Hunter, F. J. Bragg, C. Contoux, C. Stepanek, L. Sohl, N. A. Rosenbloom, W.-L. Chan, Y. Kamae, Z. Zhang, A. Abe-Ouchi, M. A. Chandler, A. Jost, G. Lohmann, B. L. Otto-Bliesner, G. Ramstein, H. Ueda, Evaluating the dominant components of warming in Pliocene climate simulations. *Clim. Past* **10**, 79–90 (2014).
52. E. Maier-Reimer, U. Mikolajewicz, T. Crowley, Ocean general circulation model sensitivity experiment with an open central American isthmus. *Paleoceanography* **5**, 349–366 (1990).
53. M. A. Cane, P. Molnar, Closing of the Indonesian seaway as a precursor to east African aridification around 3–4 million years ago. *Nature* **411**, 157–162 (2001).
54. D. J. Lunt, P. J. Valdes, A. Haywood, I. C. Rutt, Closure of the Panama Seaway during the Pliocene: Implications for climate and Northern Hemisphere glaciation. *Clim. Dyn.* **30**, 1–18 (2008).
55. X. Zhang, M. Prange, S. Steph, M. Butzin, U. Krebs, D. J. Lunt, K. H. Nisancioglu, W. Park, A. Schmittner, B. Schneider, M. Schulz, Changes in equatorial Pacific thermocline depth in response to Panamanian seaway closure: Insights from a multi-model study. *Earth Planet. Sci. Lett.* **317–318**, 76–84 (2012).
56. G. Jung, M. Prange, M. Schulz, Uplift of Africa as a potential cause for Neogene intensification of the Benguela upwelling system. *Nat. Geosci.* **7**, 741–747 (2014).
57. R. D. Garreaud, A. Molina, M. Farias, Andean uplift, ocean cooling and Atacama hyperaridity: A climate modeling perspective. *Earth Planet. Sci. Lett.* **292**, 39–50 (2010).
58. P. Sepulchre, L. C. Sloan, M. Snyder, J. Fiechter, Impacts of Andean uplift on the Humboldt Current system: A climate model sensitivity study. *Paleoceanography* **24**, PA4215 (2009).
59. Z. Liu, B. Huang, A coupled theory of tropical climatology: Warm pool, cold tongue, and walker circulation. *J. Climate* **10**, 1662–1679 (1997).
60. I. M. Held, The partitioning of the poleward energy transport between the tropical ocean and atmosphere. *J. Atmos. Sci.* **58**, 943–948 (2001).
61. N. Unger, X. Yue, Strong chemistry-climate feedbacks in the Pliocene. *Geophys. Res. Lett.* **41**, 527–533 (2014).
62. L. E. Lisiecki, M. E. Raymo, A Pliocene-Pleistocene stack of 57 globally distributed benthic $\delta^{18}O$ records. *Paleoceanography* **20**, PA1003 (2005).

63. D. C. Lang, I. Bailey, P. A. Wilson, C. J. Beer, C. T. Bolton, O. Friedrich, C. Newsam, M. R. Spencer, M. Gutjahr, G. L. Foster, M. J. Cooper, J. A. Milton, The transition on North America from the warm humid Pliocene to the glaciated Quaternary traced by eolian dust deposition at a benchmark North Atlantic Ocean drill site. *Quat. Sci. Rev.* **93**, 125–141 (2014).
64. R. A. Locarnini, A. V. Mishonov, J. I. Antonov, T. P. Boyer, H. E. Garcia, O. K. Baranova, M. M. Zweng, C. R. Paver, J. R. Reagan, D. R. Johnson, M. Hamilton, D. Seidov, *World Ocean Atlas 2013, Volume 1: Temperature* (NOAA Atlas NESDIS, 2014).

Acknowledgments: We thank H. Ford and D. Hutchinson for useful discussions on this topic and the reviewers of the manuscript for their valuable feedback. **Funding:** This research was supported by grants from the Department of Energy Office of Science (DE- SC0016538) and NSF (AGS-1405272, AGS-0163807, and AGS-1613318). N.J.B. was supported by grants from NSF (AGS-1338427), NASA (NNX14AM19G), National Oceanic and Atmospheric Administration (NA14OAR4310160), and the Alfred P. Sloan Foundation as a Research Fellow. S.L.J. was funded by the Swiss National Science Foundation (PP00P2-144811). Computations were performed at the Yale University Faculty of Arts and Sciences High Performance Computing Center. The CESM project was supported by the NSF and the Department of Energy Office of Science. **Author contributions:** N.J.B., G.H.H., A.V.F., and D.M.S. contributed equally to the writing of the manuscript. N.J.B. conducted the numerical experiments and, together with A.V.F., analyzed the results. G.H.H., S.L.J., and R.T. generated the sedimentary $CaCO_3$, biogenic opal, biomarker, trace metal, and x-ray fluorescence scanning records with other data relevant to the interpretation presented here. **Competing interests:** The authors declare that they have no competing interests. **Data and materials availability:** All data needed to evaluate the conclusions in the paper are present in the paper and/or the Supplementary Materials. Additional data from the model simulations may be requested from the authors.

Submitted 15 January 2017
Accepted 14 August 2017
Published 13 September 2017
10.1126/sciadv.1700156

Citation: N. J. Burls, A. V. Fedorov, D. M. Sigman, S. L. Jaccard, R. Tiedemann, G. H. Haug, Active Pacific meridional overturning circulation (PMOC) during the warm Pliocene. *Sci. Adv.* **3**, e1700156 (2017).

Active Pacific meridional overturning circulation (PMOC) during the warm Pliocene

Natalie J. Burls, Alexey V. Fedorov, Daniel M. Sigman, Samuel L. Jaccard, Ralf Tiedemann and Gerald H. Haug

Sci Adv **3** (9), e1700156.
DOI: 10.1126/sciadv.1700156